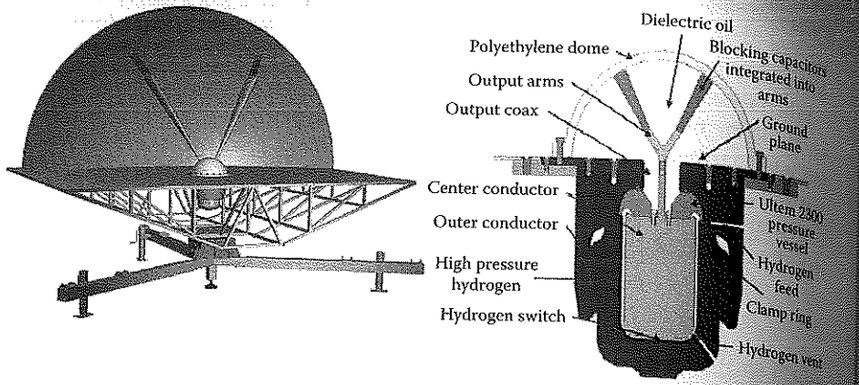

FIGURE 6.11
The MATRIX system (left) is an IRA driven by a coaxial line (right) to produce ringing oscillations. (Reprinted from Prather, W.D. et al., *IEEE Trans. EMC*, 2, 2003, Figure 1 [special issue on IEMI]. By permission of IEEE.)

6.4.1 Mesoband Systems

Mesoband sources have been successfully designed and built to generate HPM energy between 100 and 700 MHz, a range at the lower end of narrowband sources. These sources are typically designed in one of two ways:

- Feed a damped sine waveform into a wideband antenna.
- Switch a wideband transient pulse (from a Marx generator, for example) into a resonant pulse line that is connected to a UWB antenna. Pulse lines of differing lengths can be changed out to radiate a broad range of frequencies.

For the damped-sine/wideband-antenna method, Baum has described concepts that switch a high-voltage transmission line oscillator into a wideband antenna.[16] The oscillator consists of a quarter-wave section of a transmission line charged by a high-voltage source. Frequency and damping constant can be adjustable. This device employs a self-breaking switch at one end of the transmission line and the antenna at the other. When the switch closes, the system generates a damped-sine signal that is fed into a UWB antenna, such as half of an IRA. The half of a reflector over a conducting plane uses the image currents in the plane to complete the reflector. This concept makes the high-voltage problem easier, but the pattern is not the entirely symmetric field pattern of a full parabolic antenna.

For example, MATRIX is a transmission line switched into an IRA.[17] Figure 6.11 shows that it consists of a quarter-wave coaxial transmission line charged to 150 kV connected to a 3.67-m-diameter half IRA. The line, insulated by high-pressure hydrogen, is charged, then switched to ground. An

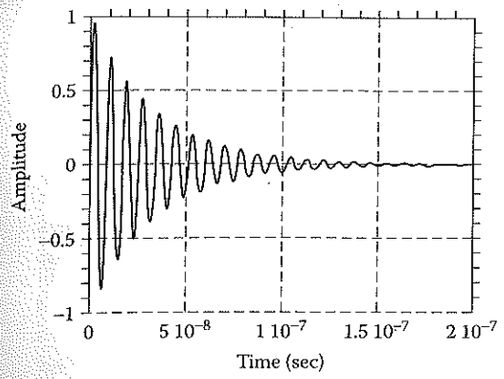

FIGURE 6.12
Calculated electric field from MATRIX at 15 m. (Reprinted from Prather, W.D. et al., *IEEE Trans. EMC*, 2, 2003, Figure 2 [special issue on IEMI]. By permission of IEEE.)

oscillation between the line and the IRA produces a damped sinusoid with frequency of oscillation that can be made adjustable between 180 and 600 MHz. Its radiated waveform is shown in Figure 6.12: a peak electric field of 6 kV/m at 15 m (figure of merit of 90 kV, gain of 0.6 at 150 kV charge) with a percentage bandwidth of about 10% (band ratio of 1.10). With a 300-kV charging supply, this source will radiate energy in the gigawatt range.

For the switched Marx/oscillating antenna method, DIEHL Munitionssysteme of Germany manufactures a number of mesoband sources.[18] One suitcase-sized version, the DS110B (for damped sinusoid), and its electric field are shown in Figure 6.13 and Figure 6.14. The DS110B operates at 750 kV, producing a peak E field of about 70 kV at 2 m (see Problem 6). It is made tunable by changing the length of the loop antenna. The repetition rate is a few hertz operating off a battery, and 100 Hz is available with a more powerful external electrical source.

Mesoband oscillators are also made by BAE Systems in the U.K.[19] These oscillators are nonlinear transmission line solid-state modulators. An example output is shown in Figure 6.15. They generate Q ~ 50 damped sine waves at ~50 kV. Frequencies range from 10 MHz to 2 GHz, with repetition rates in excess of 1 kHz. More advanced systems have the ability to chirp (increase frequency during the pulse) over a 40% range.

6.4.2 Subhyperband Systems

The H-Series systems, which use coaxial pulse-forming lines and high-pressure hydrogen switches as described in Section 6.2, were built at the Air Force Research Laboratory in Albuquerque. One of the most successful designs of the H-Series, the H-2 source, shown in Figure 6.16, is driven by a 0.1m-diameter, 40-Ω coaxial line (Figure 6.4). It generates a fast 0.25-nsec

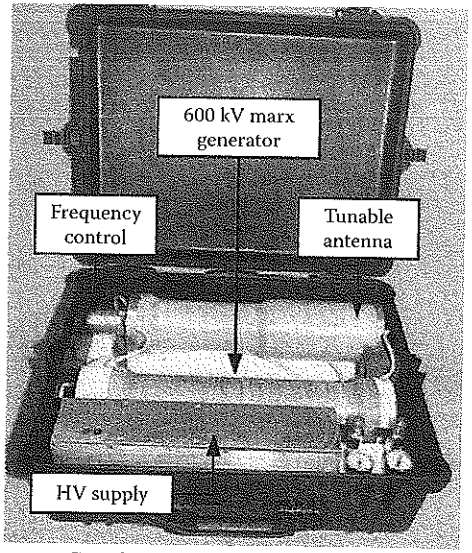

Complete DS110B high-power system

FIGURE 6.13
Suitcase-sized mesoband device, the DS110B (for damped sinusoid). (Reprinted from Prather, W.D. et al., *IEEE Trans. EMC*, 2, 2003, Figure 3 [special issue on IEMI]. By permission of IEEE.)

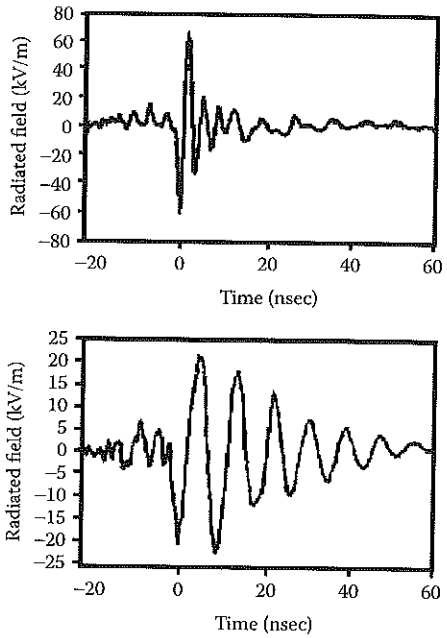

FIGURE 6.14
Tunability of the DS110B. (Reprinted from Prather, W.D. et al., *IEEE Trans. EMC*, 2, 2003, Figure 4 [special issue on IEMI]. By permission of IEEE.)

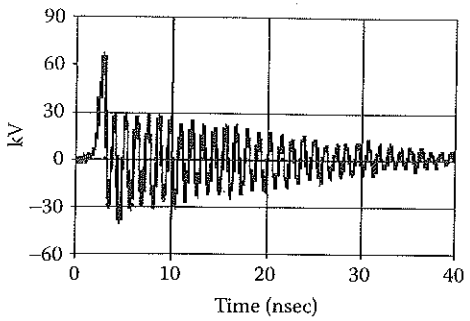

FIGURE 6.15
Voltage output from a nonlinear transmission line. (Reprinted from Prather, W.D. et al., *IEEE Trans. EMC*, 3, 2003, Figure 7 [special issue on IEMI]. By permission of IEEE.)

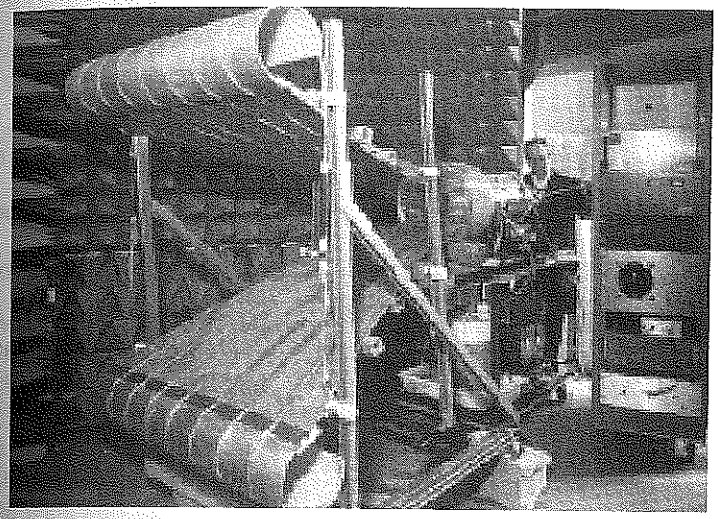

FIGURE 6.16
H-2 source with large TEM horn. (Reprinted from Prather, W.D. et al., *IEEE Trans. EMC*, 3, 2003, Figure 8 [special issue on IEMI]. By permission of IEEE.)

rise-time 300-kV pulse with a total length of 1.5 to 2 nsec and a considerable amount of late-time, low-frequency ringing. Fired into a TEM horn, the maximum spectral amplitude is at ~150 MHz. Performance is 43 kV/m at 10 m with a rise time of 0.24 nsec, very similar to that shown in Figure 6.7.

6.4.3 Hyperband Systems

The most complex and advanced sources are the hyperband, with band ratio greater than one decade. The state-of-the-art system is *Jolt*, shown in Figure 6.17.[19] The pulsed power (Figure 6.18) is a compact dual-resonant trans-

FIGURE 6.17
The Jolt apparatus. (Reprinted from Prather, W.D. et al., *IEEE Trans. EMC*, 4, 2003, Figure 13 [special issue on IEMI]. By permission of IEEE.)

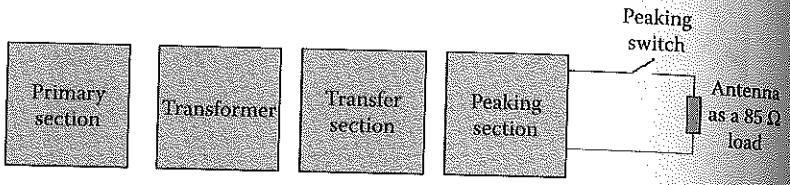

FIGURE 6.18
Jolt circuit elements. (Reprinted by permission of Giri, D.V.)

former that steps 50 kV up to 1.1 MV. A transfer capacitor leads to an oil-insulated peaking switch, which feeds an 85-Ω half IRA. The voltage rise rate is ~5×10^{15} V/sec. The ground plane below the half dish serves as the ground reference and an image plane for the IRA. It also provides the lower containment for SF6, which insulates the dome and feed arms. (For half IRAs, Equation 6.7 for the electric field is reduced by $2^{-3/2}$.)

The half-dish antenna delivers a tightly focused radiated field with a pulse length on the order of 100 psec and a field–range product of approximately 5.3 MV at 200 Hz. This is the highest figure of merit achieved in a hyperband device. The spectrum is broad, with an upper half-power point between 1 and 2 GHz and a lower half-power point around 30 MHz. The radiated waveform in Figure 6.19 has a peak field at 85 m of 62 kV and a rise time of ~0.1 nsec.

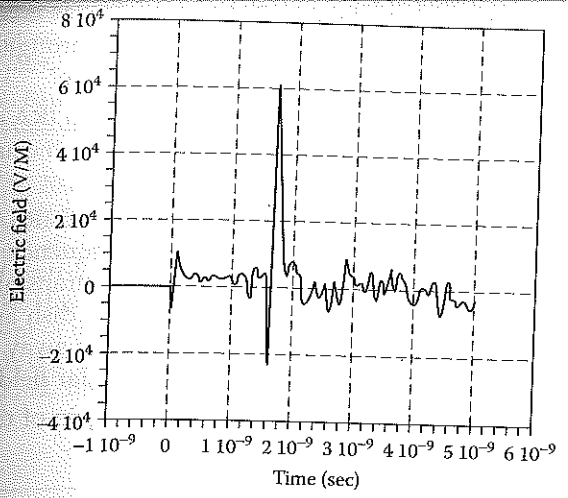

FIGURE 6.19
Measured electric field from Jolt at 85 m. (Reprinted from Prather, W.D. et al., *IEEE Trans. EMC*, 4, 2003, Figure 14 [special issue on IEMI]. By permission of IEEE.)

6.5 Conclusion

The GEM II and Jolt systems will represent the high water mark for UWB systems for some time to come. That would be parallel to the "power derby" in narrowband sources of the 1980s, which ended because of pulse shortening and cost increasing with peak power (see Chapter 1). They could find application as high power jammers for electronic warfare and short-pulse radars. The most likely direction for development of the small mesoband systems is for effects tests and directed energy, because of their compactness and low cost. Commercial versions have already reached the market for effects testing. Current technology mesoband systems operate in the 100- to 500-MHz range. Research efforts are developing devices in the 500-MHz to 1-GHz range.

Problems

1. The fractional bandwidth, percentage bandwidth, and bandwidth ratio are interrelated. Express the bandwidth ratio in terms of the percentage bandwidth. What is the maximum possible value for the percentage bandwidth?

2. How many cycles comprise a mesoband source?
3. How does the power required to drive the oil through the small dimensions of a switch gap depend on the gap size?
4. For comparison, if a narrowband source feeding an IRA operates at the upper frequency f_u, what is the relation between the narrowband and UWB far-field distances?
5. You are given a system requirement for a pulser-fed IRA to produce a figure of merit of 500 kV with an upper frequency of 2 GHz, operating down to 50 MHz. Assuming that the transmission lines are well coupled to free space ($f_g \sim 1$), what size dish antenna and what pulser voltage will be required, and how far away would you need to be to measure the figure of merit in the far field?
6. What are the resonator Q, figure of merit, and gain of the DS110B?

References

1. Giri, D.V., *High-Power Electromagnetic Radiators*, Harvard University Press, Cambridge, MA, 2004, chaps. 3–5.
2. Agee, F.J., Ultra-wideband transmitter research, *IEEE Trans. Plasma Sci.*, 26, 860, 1998.
3. Prather, W.D., Survey of worldwide high power wideband capabilities, *IEEE Trans. Electromag. Compat.*, 46, 335, 2004.
4. Giri, D.V. and Tesche, F.M., Classification of intentional electromagnetic environments (IEME), *IEEE Trans. Electromag. Compat.*, 46, 322, 2004.
5. Champney, P. et al., Development and testing of subnanosecond-rise kilohertz oil switches, in *Proceedings of the IEEE 8th Pulsed Power Conference*, San Diego, CA, 1991, p. 863.
6. Baca, A.G. et al., Photoconductive semiconductor switches, *IEEE Trans. Plasma Sci.*, 25, 124, 1997.
7. Stoudt, D.C. et al., Bistable optically controlled semiconductor switches in a frequency-agile RF source, *IEEE Trans. Plasma Sci.*, 25, 131, 1997.
8. Schoenberg, J.S.H. et al., Ultra-wideband source using gallium arsenide photoconductive semiconductor switches, *IEEE Trans. Plasma Sci.*, 25, 327, 1997.
9. Lee, C.H., Optical control of semiconductor closing and opening switches, *IEEE Trans. Electron Devices*, 37, 2426, 1990.
10. Nunnally, W.C., High-power microwave generation using optically activated semiconductor switches, *IEEE Trans. Electron Devices*, 37, 2426, 1990.
11. Prather, W.D. et al., Ultrawideband sources and antennas: present technology, future challenges, in *Ultra-Wideband, Short Pulse Electromagnetics 3*, Baum, C.E., Carin, L., and Stone, A., Eds., Plenum Press, New York, 1997, p. 381.
12. See papers in Mokole, E.L., Kragalott, M., and Gerlach, K.R., *Ultra-Wideband, Short-Pulse Electromagnetics 6*, Kluwer Academic/Plenum Press, New York, 2003.
13. http://www-e.uni-magdeburg.de/notes.
14. Giri, D.V. et al., Design fabrication and testing of a paraboloidal reflector antenna and pulser system for impulse-like waveforms, *IEEE Trans. Plasma Sci.*, 25, 318, 1997.
15. Farr, E.V., Baum, C.E., and Buchenauer, C.J., Impulse Radiating Antennas Part II, *Ultra-Wideband, Short-Pulse Electromagnetics 2*, Plenum Press, New York, 1995, p. 159.
16. Baum, C.E., 2000 Circuit and Electromagnetic System Design Note 45, Air Force Research Lab, New Mexico (see reference 14).
17. Burger, J. et al., *Design and Development of a High Voltage Coaxial Switch, Ultra-Wideband Short-Pulse Electromagnetics 6*, Plenum Press, New York, 2003, p. 381.
18. Ruffing, K., High Power Microwave and Ultra-Wideband Threats, Aspects and the Concept of the German MOD, AMEREM, 2002, Annapolis, MD.
19. Baum, C.E. et al., JOLT: a highly directive, very intensive, impulse-like radiator, *Proc. IEEE*, 92, 1096, 2004.

7

Relativistic Magnetrons and MILOS

7.1 Introduction

Crossed-field devices generate microwave energy by tapping the kinetic energy of electrons that are drifting perpendicularly to electric and magnetic fields that are oriented at right angles to one another (hence the term *crossed field*). This arrangement prevents breakdown of the anode–cathode gap, confines the electrons within an interaction region, and aligns the electron velocities with the electromagnetic waves. These devices include the *relativistic magnetron*, a high-voltage, high-current version of the well-known conventional magnetron; the *magnetically insulated line oscillator* (MILO), a linear magnetron variant that was invented to take advantage of the very high current capacity of modern pulsed power systems; and the *crossed-field amplifier* (CFA), an amplifying, rather than oscillating, near cousin of the magnetron that has been explored, but not exploited, as a high power source.

The relativistic magnetron, along with the backward wave oscillator and related devices of Chapter 8, is one of the most mature of all high power sources. The operational mechanism is robust; it is a relatively compact source; and it has been operated in the frequency range from just below 1 to about 10 GHz. It is well understood. Over the years, a number of research teams have explored the full range of operational parameters: single-source output in excess of 4 GW; multisource output in a phase-locked configuration of 7 GW total output; repetitive, near-GW peak powers at pulse repetition rates up to 1 kHz; and long-pulse operation with an energy per pulse of about 1200 J. The magnetron is the most tunable high power source, with a 30% tunable range by mechanical means, and can be tuned while firing repetitively. Theoretically, the basic design process has been understood since the 1940s, but modern computer simulation techniques have speeded the process by which major design changes are incorporated, and systems analysis has clarified the major issues involved in understanding the upper limits of achievable repetition rates and energies per pulse. Practically, the major issues of fielding a magnetron-based system have been addressed in

the Orion facility, a transportable outdoor microwave effects test system built in 1995.

The MILO has two major attractions. First, its generally low impedance — of the order of 10 Ω, about a tenth of that for a relativistic magnetron — allows for better coupling to compact, lower-voltage power sources such as explosive generators. Second, it uses the current flow in a magnetically insulated transmission line to provide the necessary magnetic field, so that no external magnet is required. Powers of 2 GW with pulse energies of about 1 kJ have been obtained, and repetition rates as high as 100 Hz, with most results obtained in the L-band. The drawbacks of this source are its lack of maturity, particularly relative to the relativistic magnetron; its lower efficiencies* of about 10%, due in part to challenges in extracting the output; and its lack of tunability. Nevertheless, commercial versions have been offered in the U.K.

Relativistic CFAs are the least mature of the high power crossed-field devices. In fact, a single very preliminary exploration of such a device based on a secondary-emission cathode was plagued with problems and terminated without achieving its original output power specification of 300 MW.

The majority of this chapter will be devoted to either the general features of crossed-field devices or the specific features of magnetrons. MILOs and, more briefly, CFAs will be treated in two sections near the end of the chapter.

7.2 History

Arthur Hull invented the magnetron in 1913, and devices built on his original principles in the 1920s and 1930s reached power levels of about 100 W. In 1940, Postumus suggested the use of a solid-copper anode, an innovation independently invented and realized also by Boot and Randall[1,2] and the Soviets Alekseev and Malairov. The initial Boot and Randall magnetron achieved 10 kW and was quickly engineered into an operational device.[3] During World War II, intense technological development of the magnetron occurred at the MIT Radiation Laboratory and other institutions, as described in Collins' classic *Microwave Magnetrons*.[4] Over the course of the war, millions of magnetrons were produced, and magnetron-driven radar probably had a greater impact on the war than any other technology invented in World War II, more so than even the atomic bomb.

Postwar development was equally fast paced into the 1960s, with the development of mode selection techniques such as strapping (shifting the frequency spectrum by connecting alternate resonators, thus preventing mode hopping) and the rising-sun geometry (alternating between two different resonator shapes to separate the modes in frequency). A new generation of higher-power, frequency-agile magnetrons was introduced for electronic warfare applications. The *coaxial magnetron* introduced by Feinstein and Collier allowed stable tuning by use of a cavity surrounding the magnetron resonator.[5] The French introduced the *magnetron injection gun*, now used extensively in gyrotrons, to drive a magnetron by a beam injected from outside the resonator. The *inverted magnetron*, with the cathode on the outside of the device and the anode on the inside, was also introduced. Gradual improvement in the understanding of magnetron operation eventually led to the *crossed-field amplifier*, in which gains of 10 to 20 dB are achieved at power levels of 1 MW or more, with amplification bandwidths of about 10%. Okress documented the state of conventional magnetron development at this time in the two-volume *Cross-Field Microwave Devices*.[6]

The relativistic magnetron was developed as a direct extrapolation of the cavity magnetron, driven at higher currents by pulsed power and cold-cathode technology. The relativistic magnetron is in fact a high-current extension of the conventional magnetron, wherein relativistic voltages are necessary to produce the currents. Bekefi and Orzechowski developed the first such devices in 1976,[7] and the most powerful was the six-vane A6, described extensively by Palevsky and Bekefi.[8] Whereas conventional devices had reached powers of about 10 MW, the first relativistic device produced 900 MW, generating great interest in the U.S. and U.S.S.R. Substantial improvements in the capabilities of magnetrons in the 1980s pushed peak powers up to several gigawatts. Frequencies extended from the original S-band device upward to the X-band and downward to the L-band. The original devices were single shot and uncooled, but cooled devices have been operated repetitively at hundreds of megawatts peak power and average powers well above a kilowatt. Microwave pulse duration is typically 30 nsec, but operation at 600 nsec has been achieved. With the generation of higher radiated energies, extending pulse durations and operating at higher average power have become principal development thrusts. In this regard, one alternative to the maximization of power in single devices has been the phase locking of multiple magnetrons together to build high power arrays of oscillators. One such array of seven magnetrons produced 7 GW of output.

Clark introduced the MILO in 1988.[9] It has the dual attractions of producing high power at low impedance, so that it couples well to lower-voltage, compact power supplies such as low-impedance explosive generators without an externally applied magnetic field. Tapered and double-MILO designs at AEA Technology in the U.K. produced relatively high efficiencies,[10] and versions are commercially available.

Some very preliminary development of high power CFAs was undertaken at the Stanford Linear Accelerator Center (SLAC) in the early 1990s. Although designed to produce 300 MW,[11] several factors limited actual CFA powers to much lower levels.

* The true comparison of efficiency, however, should take into account the electrical power demand of both the magnetron itself and its field coil, if it is an electromagnet.

7.3 Design Principles

Crossed-field devices have two distinguishing features. First, the electrons that supply the energy to generate microwaves are emitted directly from the cathode in the interaction region. No external beam-producing components are needed, so that these devices, specifically magnetrons, can be quite compact. Second, the electrons in the interaction region execute an $\mathbf{E} \times \mathbf{B}$ drift in applied electric and magnetic fields oriented at right angles to one another, with drift velocity

$$\mathbf{v}_d = \frac{\mathbf{E} \times \mathbf{B}}{|\mathbf{B}|^2} \tag{7.1}$$

Because the space-charge and diamagnetic effects of the electron layer cause $\mathbf{E}$ and $\mathbf{B}$ to vary with distance from the cathode, $\mathbf{v}_d$ does as well. The resonance requirement in crossed-field devices is that $\mathbf{v}_d$ for some electrons must equal the phase velocity of an electromagnetic wave traveling in the same direction. If z is the direction of propagation, and the wave varies in time t and z as $e^{i(kz-\omega t)}$, then resonance occurs for electrons obeying*

$$|\mathbf{v}_d| = \frac{\omega}{k} \tag{7.2}$$

The fact that the drift and phase velocities are perpendicular to both $\mathbf{E}$ and $\mathbf{B}$ distinguishes these *M-type devices*, as they are also known, from the parallel-field, or O-type, devices in which the wave propagates parallel to the applied magnetic field (see Chapter 4). Thus, crossed-field devices such as magnetrons and MILOs are M-type Cerenkov sources. Note also that the resonance condition in Equation 7.2 is the same as that for O-type Cerenkov sources in Equation 8.6.

The basic geometry of a cylindrical magnetron is shown in Figure 7.1. The main design features are the following:

- The cathode, which is separated by a gap from the anode structure. The application of a large voltage across the gap causes the explosive emission of electrons from a plasma layer created on the cold cathode (see Chapter 5).
- The interaction region between the cathode and anode, which in operation contains the drifting electrons.

* In the cylindrical geometry of magnetrons and CFAs, for a wave with azimuthal and time dependence $\exp[i(n\theta - \omega t)]$, the phase velocity on the right of Equation 8.2 is $\omega r/n$, with r within the interaction region.

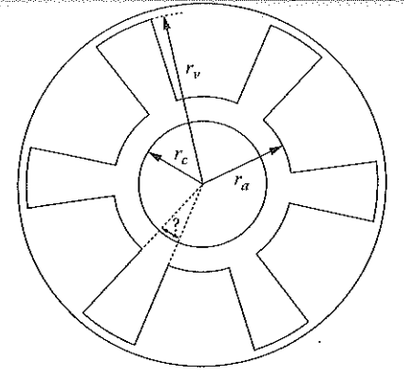

FIGURE 7.1
Basic configuration of a cylindrical magnetron: r_c and r_a are the cathode and anode radii, and r_v is the vane radius.

- The anode and the cavity structure that, together with the dimensions of the interaction region between the anode and cathode, plays the primary role in determining the operating frequencies and output modes. The axial length of the device and any cavities at the end of the device play a secondary role in determining the frequency.
- An applied axial magnetic field B_z, which must be strong enough to prevent electrons from immediately crossing the anode–cathode gap, but not so strong that the azimuthal drift velocity of the electrons, which scales roughly as $1/B_z$, is too slow to allow the resonance described in Equation 7.2.

Microwaves are extracted either *axially*, on the side opposite the pulsed power feed to the device, or *radially* from one or more of the anode cavities. The configuration of a CFA is similar in basic concept to that of a magnetron, as we can see in the schematic of Figure 7.2, which shows a coaxial CFA, with a second cavity located outside of the inner, vane-loaded microwave cavity. In detail, however, there are several additional differences in this amplifying device: microwaves are fed in through one cavity and then circulate around to be extracted at higher amplitude from another cavity; an absorbing sever between the input and output feeds prevents the microwaves from going around a second time; and the number of vanes is larger than that for many relativistic magnetrons. A MILO, depicted schematically in Figure 7.3, differs in two ways. First, it is a linear device with an azimuthal, rather than axial, magnetic field, so that the electrons and microwaves propagate axially rather than azimuthally. Second, there is no external magnetic field; the magnetic field is created by axial current flow in the device.

Electrons emitted from the cathode into the interaction region initially form a layer of electrons that drift azimuthally in the magnetron and CFA and axially in the MILO. To understand the mechanism by which electrons in

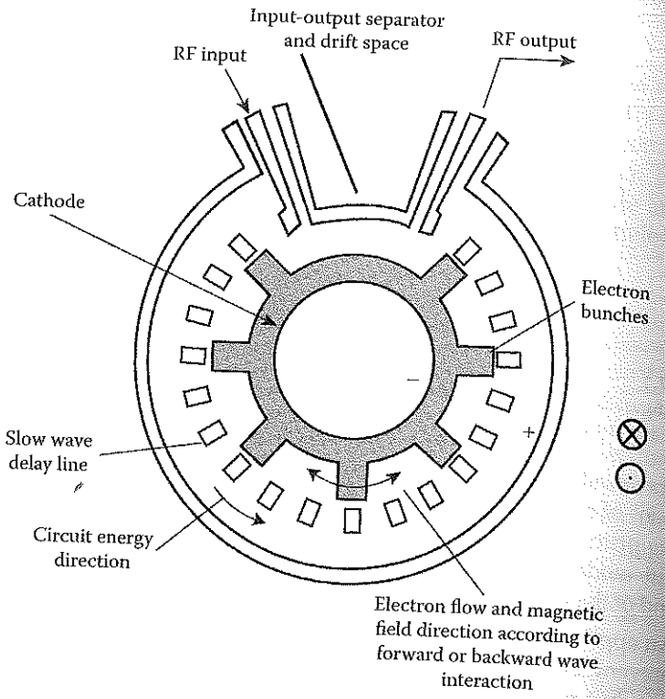

FIGURE 7.2
Schematic of the coaxial CFA investigated at SLAC. (From Eppley, K. and Ko, K., *Proc. SPIE*, 1407, 249, 1991. With permission.)

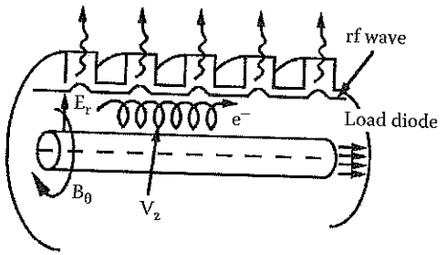

FIGURE 7.3
Schematic of a MILO indicating the drift of a single electron from the cathode sheath and its net axial drift in the radial electric field and azimuthal magnetic field. Radial extraction is shown here, although axial extraction has become more common.

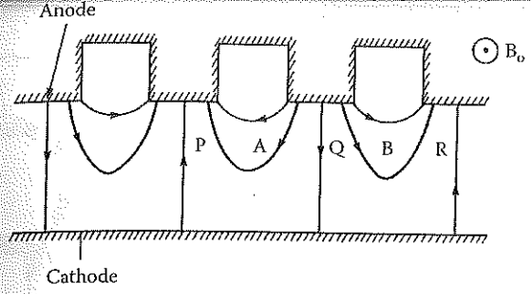

FIGURE 7.4
Behavior of test electrons in the π-mode electric fields of magnetrons and CFAs. (From Lau, Y.Y., *High-Power Microwave Sources*, Artech House, Boston, 1987, p. 309. With permission.)

this layer transfer their energy to the microwaves, consider the two test electrons in Figure 7.4, labeled A and B.[12] For simplicity, the geometry is planar and the microwave fields are those of the π-mode, which reverses phase from one cavity to the next. To be resonant, the electromagnetic wave has a phase velocity that is about the same as the initial drift velocity of the electrons. To start with, both electrons execute $\mathbf{E}_0 \times \mathbf{B}_0$ drifts in which the forces due to the applied electric and magnetic fields cancel. The combination of the microwave electric field component, $\mathbf{E}_1$, and the applied magnetic field, $\mathbf{B}_0$, affects each electron in four ways. First, $\mathbf{E}_1$ decelerates A and accelerates B. Second, $\mathbf{E}_1 \times \mathbf{B}_0$ pushes A toward the anode and B away from the anode. Third, since the microwave fields are stronger near the slow-wave structure at the anode, A is decelerated even more near the anode, while B is accelerated less as it approaches the smooth cathode. Fourth, as A approaches the anode, it loses potential energy, which is converted to microwave energy, while B gains potential energy, which is supplied by the microwave field energy. Because these effects are stronger for A than for B, more energy is delivered to the microwave fields than is drawn from them, and the fields grow in magnitude.

In concert with the basic gain mechanism, a second phenomenon, *phase focusing*, enhances the gain and leads to the formation of the spokes shown in Figure 7.5, which is taken from computer simulations of the rotating spoke patterns for the A6 magnetron operating in the π- and 2π-modes.[13] To understand phase focusing, return to Figure 7.4 and imagine first that electron A has a drift velocity larger than the phase velocity of the microwave fields. When it advances to location P, where E_{r1} opposes E_{r0}, its drift velocity $(E_{r0} + E_{r1})/B_z$ is reduced, and the drift velocity falls back toward synchronism with the wave. Conversely, if A drifts more slowly with the wave, when it drops back to Q, where the microwave field reinforces the applied field, the drift velocity increases, and A moves back toward synchronism. By this same reasoning, we can see that if the drift velocity of electron B is faster than that of the wave, its velocity increases still further when it reaches Q, and if it drifts more slowly than the wave, its velocity tends to decrease even further

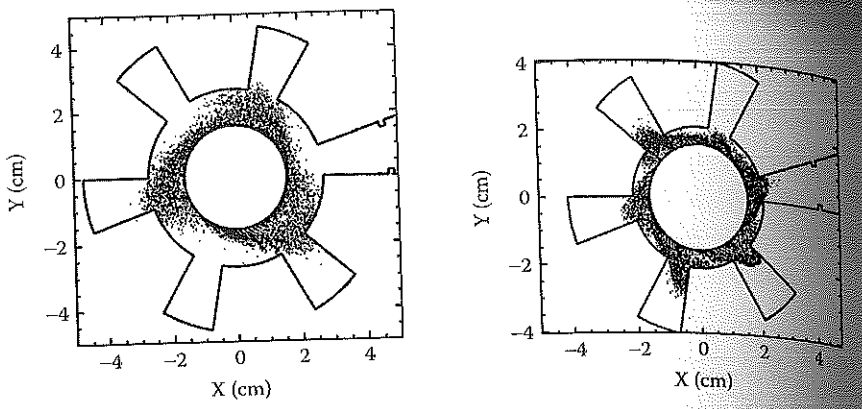

FIGURE 7.5
Spoke patterns from simulations of the A6 magnetron: (a) π-mode operation, with spokes every other cavity (in this snapshot of a rotating pattern); and (b) 2π-mode operation, with spokes at every cavity (again, in a snapshot of a rotating pattern). (From Lemke, R.W. et al., *Phys. Plasmas*, 6, 603, 1999. With permission.)

when it drops back to R. Thus, resonant electrons such as A, which supply energy to the fields, are held in synchronism with the wave, while electrons such as B, which draw energy from the fields, are defocused in phase from the wave.

The spokes carry electrons across the gap, and this radial current flow completes the circuit for an axial current flow through the device. This axial current flow creates an azimuthal magnetic field that, in concert with the radial electric field, creates an axial component of electron velocity. Electrons are thus lost to the anode via the spokes and to the ends of the magnetron via the drift the axial current creates. The locations of loss must be found if x-ray shielding and cooling are required.

In the remainder of this section we address three primary design issues, focusing primarily on the magnetron, although much of the discussion is relevant to its close relative, the CFA:

1. The cold frequency characteristics determined by the configuration of the interaction region and anode cavities (i.e., in the absence of the electrons), which are quite accurate even with the addition of electrons
2. The relationship between the applied voltage and magnetic field, determining where in a parameter space of these two variables is device breakdown prevented and microwave generation allowed
3. The behavior of the device with electrons included, which must largely be done using empirical data and computer simulation because of the highly nonlinear behavior of the operating device

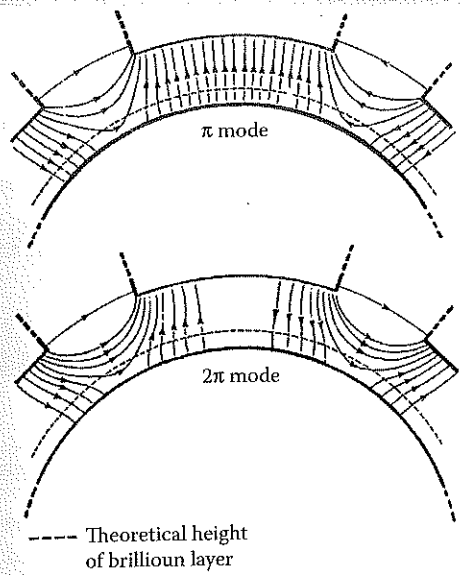

FIGURE 7.6
RF electric field patterns for the (a) π- and (b) 2π-modes. (From Palevsky, A. and Bekefi, G., *Phys. Fluids*, 22, 986, 1979. With permission.)

7.3.1 Cold Frequency Characteristics of Magnetrons and CFAs

The coupled resonators of the anode surrounding the annular interaction region between the cathode and anode create a variety of potential operating modes for the magnetron, each with its own characteristic operating frequency and microwave field pattern. Magnetron modes are designated by mode number n for fields that vary azimuthally as $e^{in\theta}$; n is thus the number of times the microwave field pattern repeats during a circuit around the anode. Since the angular spacing between N cavities is $\Delta\theta = 2\pi/N$, the phase shift between adjacent cavity resonators for the nth mode is $n\,\Delta\theta = 2\pi n/N$ (see Problems 3 to 5). In magnetrons, there are two common operating modes: the *π-mode*, wherein the fields are reversed from one cavity to the next ($n = N/2$, $\Delta\theta = \pi$), and the *2π-mode*, with fields repeating from cavity to cavity ($n = N$, $\Delta\theta = 2\pi$). The electric fields for the π- and 2π-modes of the A6 magnetron (N = 6) are shown in Figure 7.6.[8] For further discussion of magnetron mode structure, see Treado.[14]

The dispersion relation for a magnetron relates the frequency for a given mode, ω_n, to either n or the phase shift per cavity, Δθ. In the case of a magnetron or CFA, it is usually calculated numerically with an electromagnetic field code or analytically using the technique described in Collins' book.[4] The dispersion relation for magnetrons was discussed in detail in Section 4.4.2. Figure 7.7 shows the dispersion relation for the A6 magnetron,[8] with N = 6 and cathode and anode radii of $r_c = 1.58$ cm and $r_a = 2.11$ cm; the

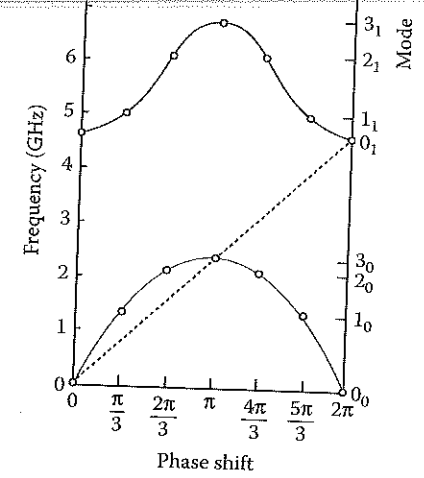

FIGURE 7.7
Dispersion relation, $f_n = \omega_n(\Delta\theta)/2\pi$, for the A6 magnetron. The azimuthal phase velocity of the π- and 2π-modes are the same, although this occurrence is coincidental.

anode cavities have azimuthal opening angles of $\psi = 20°$, and the cavity side walls extend along radial lines to a depth of $r_d = 4.11$ cm, measured from the center of the device. The peak frequency for the modes on the lowest-order curve is the π-mode frequency, about 2.8 GHz. All other modes in that set are doubly degenerate in frequency. The 2π-mode is the lowest-frequency mode in the second-order mode set. The slope of a line drawn from the origin defines the angular phase velocity of a mode. Note that for the A6, the π- and 2π-modes have the same phase velocity; however, they have different Buneman–Hartree conditions (discussed in the next subsection) and field patterns, and therefore are easily separated in practice.

In Collins' book, graphical solution of the dispersion relation reveals that the π-mode frequency lies somewhat below the frequency for which the length of the anode cavities $L_a = r_v - r_a$ is approximately $\lambda/4$, with λ the free-space wavelength of the output radiation. Therefore,

$$f_\pi = \frac{\omega_\pi}{2\pi} = \frac{c}{\lambda} \approx \frac{c}{4L_a} \tag{7.3}$$

In the case of the A6 magnetron, Equation 7.3 yields $f_\pi \approx 3.75$ GHz, which is high by about 60%. This rule of thumb is at least helpful for scoping calculations with somewhat better than factor-of-two accuracy. Further, it points to the relevant scaling parameter for the π-mode frequency.

Magnetrons also have an axial mode structure, particularly when the resonator is shorted at the ends by conducting end caps, or even when it is open on the ends, but its length is not large in comparison to the gap. Under

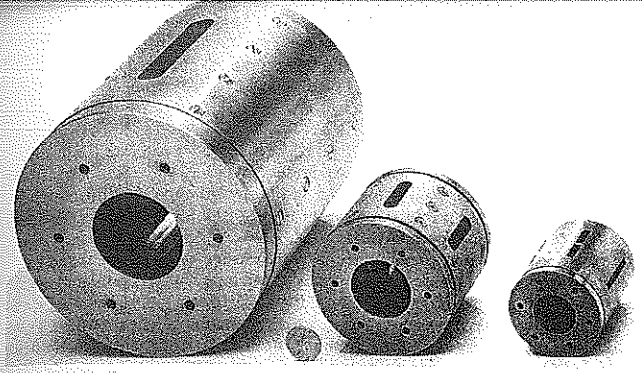

FIGURE 7.8
L-, S-, and X-band magnetrons, compared to a U.S. penny. (Courtesy of L-3 Communications Pulse Sciences, formerly Physics International.)

these circumstances, the frequency of a given mode is modified by the axial modes according to the relation

$$\left(f_n^g\right)^2 = \left(f_n^0\right)^2 + \left(\frac{gc}{4h}\right)^2, \; g = 1, 2, 3, \ldots \tag{7.4}$$

where h is the resonator length. Clearly, mode competition will be an issue if $h > \lambda$. Typical experimental values for the resonator length are ~0.6 λ, although relativistic magnetrons with $h = 2\lambda$ have been reported in the X-band.[15] Competition among axial modes frequently limits output power in experiments. The most easily observed symptom is beating of the power pulse at the difference frequency, $\Delta f = f_n^{g+1} - f_n^g$.

According to Equations 7.3 and 7.4, the size of a magnetron scales inversely with the operating frequency f, or directly with the free-space wavelength λ. Figure 7.8 allows one to compare the resonator sizes for magnetrons operating in different frequency bands between roughly 1 and 10 GHz. In Table 7.1, for a number of U.S. magnetrons,[14,16,17] we compare the radii of the cathode, anode, and the anode resonator — r_c, r_a, and r_v — as well as the resonator length h, to λ; we also show the π-mode frequency estimated using Equation 7.3 for those devices that operate in that mode (see Problem 6). For the noninverted magnetrons (i.e., those with $r_c < r_a$), we can see that r_c typically ranges between one eighth and one fifth of a wavelength, with the PI L-band magnetron an outlier at $r_c = 0.05\lambda$; r_a ranges from one sixth to about one third λ, with the PI X-band magnetron an outlier on the high end and the PI L-band magnetron an outlier on the low end. The estimate of the π-mode operating frequency in Equation 7.3 is always high, by as much as 60% in a couple of the MIT magnetrons to as little as 6% in the PI X-band device. Resonator lengths are typically a fraction of a wavelength, but the length is almost twice λ in the PI X-band device. We